






Enhancement of electron-impact ionization induced by warm dense environmentsPing Zhang ¹, Yang Jin,¹ Xiaolei Zan ¹, Pengfei Liu,⁴ Yongjun Li ¹, Cheng Gao,¹ Yong Hou ^{1,*},
Jiaolong Zeng,^{2,1,†} and Jianmin Yuan ^{3,1,‡}¹*Department of Physics, College of Liberal Arts and Sciences, National University of Defense Technology, Changsha Hunan 410073, People's Republic of China*²*College of Science, Zhejiang University of Technology, Hangzhou Zhejiang 310023, People's Republic of China*³*Graduate School, China Academy of Engineering Physics, Beijing 100193, People's Republic of China*⁴*College of Advanced Interdisciplinary Studies, National University of Defense Technology, Changsha Hunan 410073, People's Republic of China*

(Received 12 July 2021; revised 9 August 2021; accepted 27 August 2021; published 13 September 2021)

Studies have shown significant discrepancies between the recent experiment [Berg *et al.*, *Phys. Rev. Lett.* **120**, 055002 (2018)] and current theoretical calculations on the electron-impact ionization cross section of ions in warm dense magnesium. Here, we present a systematic study the effects of the ionic correlations and free-electron screening on the electron-impact ionization of ions in warm dense matter. The ionic correlation and the free-electron screening effects yield additional Hermitian terms to the calculation of the ionic central-force-field potential, which significantly change the electronic structure compared with that of the isolated ion. In calculating the electron-impact ionization, we describe the impact and ionized electrons using a damped-distorted wave function, which considers the momentum relaxation of free electrons due to collisions with other free electrons and ions. We reproduce the electron-impact ionization process for Mg^{7+} in the solid-density plasma and increase the ionization cross section by one order of magnitude compared with that of the isolated ion, which excellently agrees with the experimental result of Berg *et al.*

DOI: [10.1103/PhysRevE.104.035204](https://doi.org/10.1103/PhysRevE.104.035204)**I. INTRODUCTION**

Recently, the development of laser technology has seen the production of warm dense matter using ultra-intense lasers in the laboratory [1–6], thus promoting the rapid development of studies in high-energy-density physics [7,8]. The electron-impact ionization process can be used to infer the charge-state distribution, the electron temperature, and density of plasmas [9–11] that is crucial for both fundamental science and practical applications in modeling of concepts in astrophysics and laboratory plasmas [12–14]. However, the measurement of Berg *et al.* [15], which studied how charge states generated using electron-impact ionization process via resonance pumping of the $1s$ - $2p$ transition significantly differs from theoretical calculations on the electron-impact ionization cross section in warm dense matter. The experimental result is larger than the predicted values from the standard atomic-collision theory, which provides some new insights into ionization in warm dense matter.

Until now, most calculations of the electronic structure are based on isolated atoms or ions [16–18]. These methods neglect ionic strong coupling and electronic degeneracy and only apply to rarefied plasmas. However, when the plasma density is high that the ionic coupling cannot be neglected, the ion-ion

correlation plays an important role. The Debye-Hückel (DH) model [19–21] is widely used to calculate several electronic data in strongly coupled plasma, however, it only considers the screening of free electrons around ions and does not adequately describe the dense environment. Starrett *et al.* [22–24] considered the interactions with other ions and surrounding free electrons using the correlation functions in calculating the ionic central-force-field potential. Hou *et al.* also applied the theoretical method in the average-atom (AA) code to calculate both the ionic and electronic structures [25] and the x-ray Thomson scattering (XRTS) [26,27], which are in good agreement with the experimental results.

For calculating the isolated electronic structure in the central-force-field potential, the scattered electron is described using the distorted plane wave in the electron-impact ionization process, which is also applicable to low-density plasmas. The collision process is described as a time-independent static process. More so the final states of the scattered electrons are assumed to be influenced by only the central-force-field potential of the target ion, independent of other ions and surrounding free electrons. This implies that the contribution from free-electron collisions with surrounding free electrons and ions is neglected and is called multiple scattering in Refs. [28–31]. However, it breaks down in warm dense matter where the free-electron-collision events play an important role, especially for the near-threshold free electron. Thus, the momentum no longer becomes a constant due to the collision of surrounding free electrons and ions [30], leading to the momentum having varying relaxation

*yonghou@nudt.edu.cn

†jlzeng@zjut.edu.cn

‡jmyuan@nudt.edu.cn

times. Additionally, the scattered electron becomes partially dephased compared with the distorted plane wave [32], reflecting the time-dependent dynamic evolution of the wave function. Kuchiev and Johnson [29,30] proposed that the wave function of the near-threshold free electron can be modified by using the damped-distorted plane wave, such that the decay factor is related to the relaxation time.

This study obtains the electronic structure including the ionic and electronic correlation effects in warm dense matter and calculates the electron-impact-ionization cross section by adding damping of the final state to explain the discrepancies between experimental and present theoretical results. First, we calculate the electronic structures using the modified flexible atomic code (FAC) [33], such that the effects of ionic and electronic correlations are included in the self-consistent potential, and the correlation functions are obtained using the hypernetted-chain approximation. Following the self-consistent calculations, the ionization potential depression (IPD) effect is considered according to the two-step method of Son *et al.* [34]. Then, the damped-distorted plane wave [29,30] is used for scattered electrons, where the collision frequency is computed using the Born-Mermin approximation (BMA) [35]. Finally, taking the solid-density magnesium as an example, we calculate the electron-impact ionization cross section of Mg^{7+} at a free-electron density of $3 \times 10^{23} \text{ cm}^{-3}$ and a temperature of 75 eV.

II. THEORY

A. Electronic structure calculations including the free-electron and ionic correlation effects

The cross section of the electron-impact ionization depends on the electronic structure. Here, we obtain the electronic structure using the modified flexible atomic code (FAC) [33], which solves the Dirac equation in the central-force-field potential of atom or ion:

$$\left(\frac{d}{dr} + \frac{\kappa}{r}\right)P_{n\kappa}(r) = \alpha \left[\varepsilon_{n\kappa} - V(r) + \frac{2}{\alpha^2} \right] Q_{n\kappa}(r), \quad (1)$$

$$\left(\frac{d}{dr} - \frac{\kappa}{r}\right)Q_{n\kappa}(r) = \alpha [-\varepsilon_{n\kappa} + V(r)]P_{n\kappa}(r), \quad (2)$$

where $P_{n\kappa}(r)$ and $Q_{n\kappa}(r)$ are the large and small components of the wave function, respectively, α is the fine-structure constant, $\varepsilon_{n\kappa}$ is the energy eigenvalue of the orbital $n\kappa$, and $V(r)$ is a self-consistent potential. In warm dense matter, the correlation effects between charged ions are non-negligible because of the strong coupling, which changes the self-consistent potential compared with isolated atoms or ions. So our approach combined the ionic and free-electron correlation effects in the FAC to calculate the electronic structure of the form [24,26,27]

$$\begin{aligned} V(r) = & -\frac{Z}{r} + \int \frac{\rho_b(r')}{|\vec{r} - \vec{r}'|} d^3 r' + V_{xc}[\rho_b(r) + \rho_e^0] - V_{xc}[\rho_e^0] \\ & - \frac{\rho_e^0}{\beta} \int C_{ee}(|\vec{r} - \vec{r}'|) h_{ie}(r') d^3 r' \\ & - \frac{\rho_i^0}{\beta} \int C_{ie}(|\vec{r} - \vec{r}'|) h_{ii}(r') d^3 r'. \end{aligned} \quad (3)$$

The first line has contributions from single ions, namely, the electron-nuclear Coulomb potential, electrostatic Coulomb-repulsion potential with the other bound electrons, and the exchange and correlation potential, evaluated with the local density approximation (LDA) [36]. The second and third lines in Eq. (3) represent the ionic and electronic correlations, that is, the interactions of electrons with other free electrons and ions, respectively. Obtaining $V(r)$ requires the bound-electron density $\rho_b(r)$ and correlation functions. The radial distribution of the bound-electron density is computed as

$$\rho_b(r) = \frac{1}{4\pi r^2} \sum_j l_j [P_j^2(r) + Q_j^2(r)], \quad (4)$$

where l_j is the occupation number of bound state j . By knowing the correlation functions, Eqs. (1) and (2) can be solved self-consistently to obtain the electronic structure. Furthermore, the free-electron density $\rho_f(r)$ in momentum space can be obtained using the Thomas-Fermi (TF) approximation [37,38]. And $\rho_{\text{tot}}(r) = \rho_b(r) + \rho_f(r)$ is the total electron density in the ion sphere, and the chemical potential guarantees electrical neutrality

$$\int_0^{R_{ws}} 4\pi r^2 \rho_{\text{tot}}(r) dr = Z, \quad (5)$$

where Z is the nuclear charge, R_{ws} is the ion-sphere radius, computed as $R_{ws} = (3/4\pi n_i)^{1/3}$, and n_i is the ion number density of warm dense matter. The ion-electron total correlation function [24] is defined using the excess free-electron density as

$$h_{ie}(r) = \frac{\rho_f(r)}{\rho_e^0} - 1, \quad (6)$$

where ρ_e^0 is the uniform electron density, given by the total electron density at the boundary R_{ws} of the ion sphere $\rho_e^0 = \rho(R_{ws})$. Then, using the HNC approximation, known to be suitable for strong-coupling system [39–43] we calculate the correlation function

$$h_{ab}(r) = \exp[-\beta V_{ab}(r) + h_{ab}(r) - C_{ab}(r)] - 1, \quad (7)$$

where a and b denote the electron or ion, and the direct correlation function $C_{ab}(r)$ is connected to the total correlation $h_{ab}(r)$ using the Ornstein-Zernike relation [39]

$$h_{ab} = C_{ab} + \sum_c n_c \int d\vec{r}' C_{ac}(\vec{r}-\vec{r}') h_{cb}(|\vec{r}-\vec{r}'|), \quad (8)$$

where n_c represents the number density of type- c particle. Our calculation considered the pair potential between ions using the Yukawa model [44–46] where the inverse of screening length is computed using the Fermi integral function of free electrons. Since the interaction between ions in warm dense matter is mainly screened by free electrons, we only investigated the contribution of free electrons. Furthermore, we applied the Deutsch potential [41] in calculating the pair potential between free electrons. Also, quantum effects, such as the uncertainty principle and exchange interactions, temperature dependence are included in the Deutsch potential.

B. Electron-impact-ionization cross section

In the electron-impact-ionization process, the cross-section from an initial state ψ_i to a final state ψ_f can be expressed as [47]

$$\frac{d\sigma_{if}(\varepsilon_0, \varepsilon)}{d\varepsilon} = \frac{2\pi}{k_i^2 g_i} \sum_{\kappa_i, \kappa_{f1}, \kappa_{f2}} \sum_{J_T} (2J_T + 1) \left| \langle \psi_i \kappa_i, J_T M_T | \right. \\ \left. \times \sum_{p < q} \frac{1}{r_{pq}} | \psi_f \kappa_{f1} \kappa_{f2}, J_T M_T \rangle \right|^2, \quad (9)$$

where k_i and ε_0 are the kinetic momentum and energy of the incident electron, respectively, and k_i is related to the energy ε_0 by $k_0^2 = 2\varepsilon_0(1 + \frac{\alpha^2}{2}\varepsilon_0)$. ε is the energy of the ejected electron, g_i is the statistical weight of the initial state, κ_i , κ_{f1} , and κ_{f2} denote the relativistic angular quantum numbers of the incident, scattered, and ejected electrons, respectively. J_T is the total angular momentum when the final state is coupled to the ejected electron, and M_T is the projection of the total angular momentum. The energy reservation $\varepsilon_0 = I + \varepsilon_1 + \varepsilon$ holds for the ionization process, here I is the ionization potential and ε_1 is the energy of scattered. The total cross section is obtained by integrating over the energy ε of the ejected electron [47].

By considering the result of the high-frequency collisions with other ions and free electrons in the strong damping of the scattered electron wave function, then the wave functions of the scattered electron using the damped-distorted plane wave are defined according to Ref. [30]:

$$\Psi_p(r, t) = \psi_p(r) \exp(iE_p t - t/\tau_p), \quad (10)$$

where $\psi_p(r)$ is the distorted wave function, and τ_p represents the lifetime (relaxation time) of the state, which is the inverse of the collision frequency $\nu(\omega)$ obtained using BMA [35]. When we calculate the corresponding time-independent wave functions, the term, t/τ_p , leads to additional imaginary phase shift of the radial part wave function [28] and can be replaced by $r\nu(\omega)/\bar{v} = r/\bar{l}$ in the distorted wave function, where \bar{l} is the mean-free path. So in the electron-impact-ionization cross section the distorted wave function, $\psi_p(r)$, is replaced by the damped-distorted wave function, $\psi_p(r) \exp(-r/\bar{l})$.

III. RESULTS AND DISCUSSION

A. The influence of the free-electron and ionic correlation effects on atomic structure

The electron-impact ionization cross section depends on the electronic structure and scattering matrix in terms of Eq. (9). To consider the influence of the warm dense environment on the electronic structure, the central potential $V(r)$ including the ionic and free-electron correlation effects is obtained for Mg^{7+} at a temperature of 75 eV with different densities using the modified FAC. The results are shown in Fig. 1. When r is larger than R_{ws} , $V(r)$ becomes the constant value ε_s at the boundary of the ion sphere. An increase in the plasma density, a decrease in $V(r)$ at their respective ion-sphere boundaries. So the absolute value of ε_s becomes larger, as with the ionic center potential in solids due to including the ionic correlations. With the density decreasing, $V(r)$ gets closer to that of the isolated ion. Here, the cor-

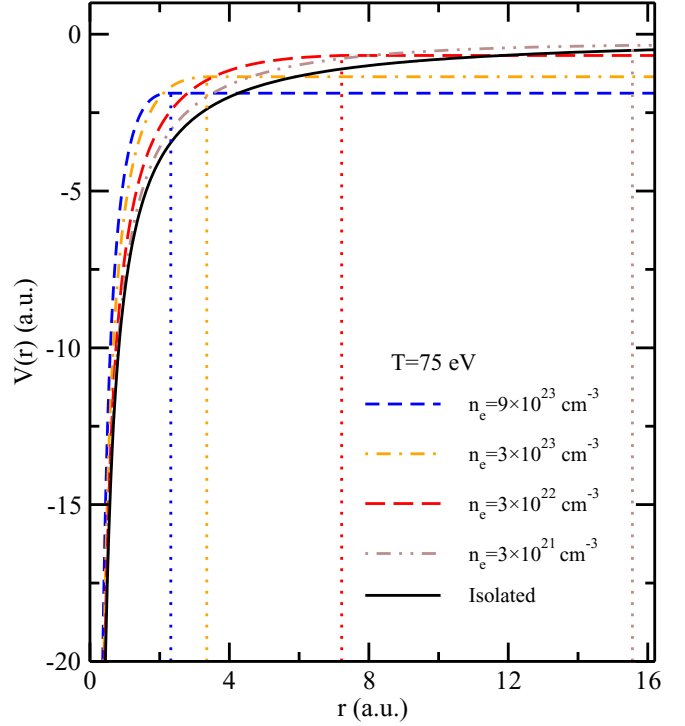


FIG. 1. The central-force-field potential of Mg^{7+} ion at a temperature of 75 eV. The black solid line represents the result at the boundary condition of the isolated ion, brown dot-dot-dashed, red long-dashed, orange dot-dashed, and blue short-dashed lines represent the results, including the ionic and free-electron correlation effects on the central-force-field potential at four free-electron number densities, namely, 3×10^{21} , 3×10^{22} , 3×10^{23} , and $9 \times 10^{23} \text{ cm}^{-3}$, respectively. The dotted lines represent the positions of the ion-sphere radius, $R_{ws} = (3/4\pi n_i)^{1/3}$, for different densities, including 15.56, 7.22, 3.35, and 2.32 in atomic units, respectively.

relation functions of the electron-ion and electron-electron are used to describe free-electron screening effects, which is different from other screening models [32,34,48]. Also, the ionic correlation makes the potential change at the boundary of ionic sphere. So the effects of the ionic and free-electron correlations yield an additional Hermitian potential, changing of the central potential, especially for high-density plasma.

In the self-consistent calculations using the modified FAC [33], the radial wave functions of the bound electrons are obtained at the same conditions, as shown in Fig. 2. The radial wave functions for low-density plasmas hardly changed compared with that of the isolated ion for all different shells. With an increasing in density, the radial wave functions expanded more to outward because the ionic and free-electron correlation effects become more important. Noticeably, results for the highest density vary, $9 \times 10^{23} \text{ cm}^{-3}$. From the figure, the variation of the radial wave functions of the inner-shell electrons, such as $1s$ and $2p$ electrons in Figs. 2(a) and 2(b), can be neglected for all different-density plasmas. However, the results of both $3s$ and $3d$ electrons show that the expansions are more significant in Figs. 2(c) and 2(d). Furthermore, the distributions of outer-shell electrons become more near the ion-sphere boundary and are more susceptible to the external environment. When considering the orbital energy of the

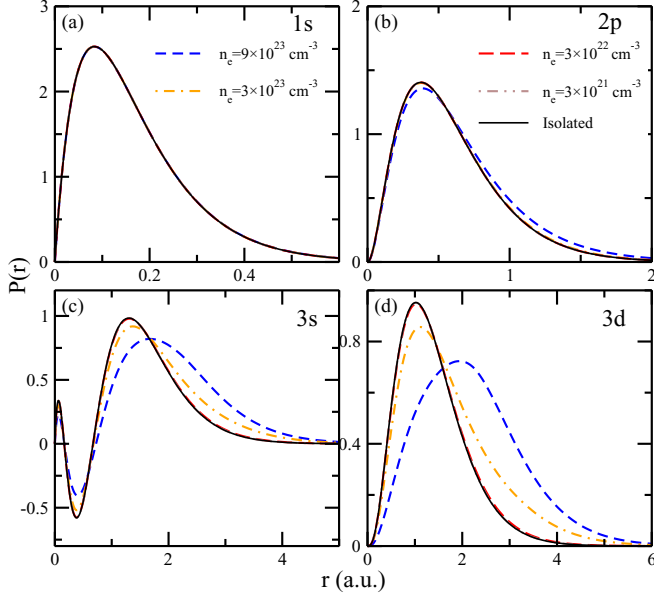


FIG. 2. Radial wave functions of 1s, 2p, 3s, and 3d electrons of Mg⁷⁺, as shown in panels (a)–(d), respectively. The black solid lines are computed at the boundary condition of the isolated ion, the other results are calculated from the central-force-field potential, as shown in Fig. 1.

outer shell electrons, such as the 3d electron in Fig. 2(d), the changes relative to its orbital energy and radial wave function are the greatest and most obvious, respectively.

Besides that the bound electronic structures are influenced by the warm-dense environment, the multiple scattering process results in the momentum of the free electron only exists finite period of time due to collisions with ions and other free electrons [28]. The scattered electron in the electron-impact-ionization process are described using the damped-distorted wave function in the central-force-field potential of the target ion [30]. To show the difference from other wave functions, three wave functions are calculated at the temperature of 75 eV and three densities in Fig. 3. The black dashed lines denote the results of distorted plane wave at the isolated-ion boundary condition. And the results, including the ionic and free-electron correlation effects, are labeled with the blue dot-dashed lines. The blue dot-dashed lines move outwards compared with the black dashed lines. For low-density plasma in Fig. 3(a), moving is trivial, especially near the nucleus shown. As the free-electron density increases, the change of wave function becomes greater, as shown in Figs. 3(b) and 3(c). From the results of including ionic and free-electron correlation effects, we consider the dissipation using the decay factor and calculate the damped-distorted wave function represented in red solid lines using Eq. (10). The amplitude of the wave function gradually decays as the radial distance r increases due to collision with other free electrons, and the collision frequency increases with the increase in density and temperature. Therefore, the dissipation mechanism becomes stronger and the amplitude of the wave function decays faster at higher densities, as shown in Fig. 3(c).

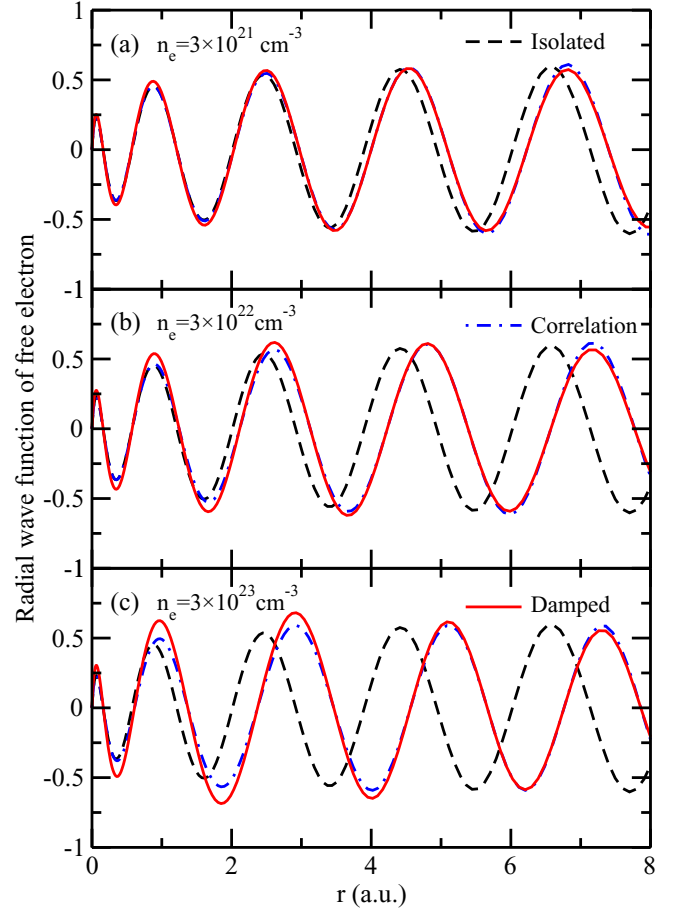


FIG. 3. The free-electron wave function with the energy of 75 eV are given using three models at a temperature of 75 eV and different densities of 3×10^{21} , 3×10^{22} , and $3 \times 10^{23} \text{ cm}^{-3}$, as shown in panels (a)–(c), respectively.

B. Ionization potential depression

The ionic and free-electron correlation effects shift the energy level of the atom in warm dense matter, resulting in the ionization potential depression (IPD) [49–57]. Here, the IPD is calculated by using the two-step model [34]. First, the orbital energy ε_{iso} and wave function of the bound state is obtained at the isolated-ion boundary condition using FAC, then the ionization potential, V_{iso} , is computed using $0 - \varepsilon_{\text{iso}}$. Second, the orbital energy ε_{env} is obtained similarly, and the ionic and free-electron correlations are included in the Hamiltonian to examine the influences of other ions and free electrons. At the ion-sphere boundary, the potential is labeled ε_s . When the energy of the electron $\varepsilon > \varepsilon_s$, the electron is no longer bound in the ionic potential well and becomes quasicontinuous. So we obtain the ionization potential using the formula V_{env} as $\varepsilon_s - \varepsilon_{\text{env}}$. Finally, by comparing with V_{iso} , the IPD of the ion embedded in the warm dense environment is computed using

$$I_{\text{ipd}} = V_{\text{iso}} - V_{\text{env}} = \varepsilon_{\text{env}} - \varepsilon_{\text{iso}} - \varepsilon_s. \quad (11)$$

To check the self-consistent calculation for IPD, we calculated different charge states Mg^{*n+*} at the free-electron density of $3 \times 10^{23} \text{ cm}^{-3}$ and temperature of 75 eV using Son's two-step model [34], as shown in Fig. 4, and compare with the

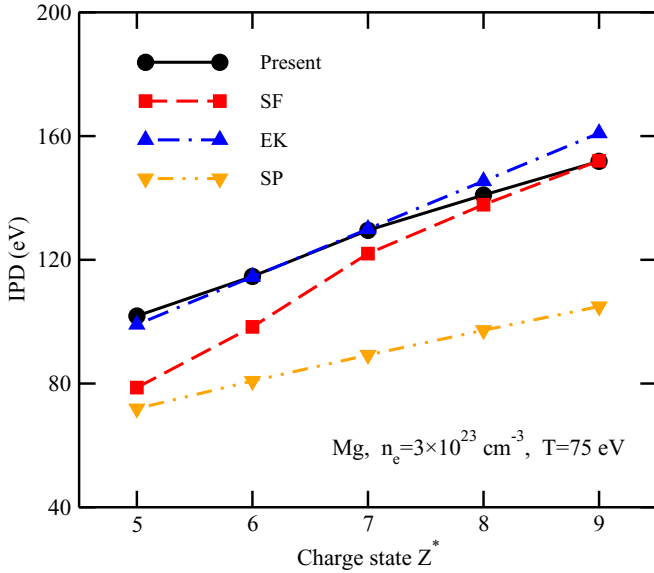


FIG. 4. IPD results of Mg^{n+} at the free-electron density of $3 \times 10^{23} \text{ cm}^{-3}$ and temperature of 75 eV. The black solid line with circles is present results calculated by two-step model based on the modified FAC. The red dashed, blue dot-dashed, and orange dot-dot-dashed lines are the results of the SF, EK, and SP models, respectively.

results of Ecker and Kröll (EK) [52], Stewart and Pyatt (SP) [53], and the structure factor (SF) [58] theoretical models. The EK model uses the effective screening length to describe the IPD and considers the ion and free electron to give same contribution, and the effective screening length depends on the sum of ionic and free-electron densities. The SP model extends it to the study of weakly coupled plasmas, which only uses the ion average distance to consider effective screening. From Fig. 4, we can see that our results increase with an increase in the charge state, and charge states 5, 6, 7, and 8 are very close to that of the EK model and charge state 9 is more close to that of SF models. The EK model gives reasonable results in the strongly coupled regime, as does the SP model for the weak-coupled plasma. To include the dynamic screening effect, Lin *et al.* [54–56] developed the SF model using the dynamic structure factor (DSF). Recently, we extended this model by including the local field correction for DSF [58] from the atomic structure calculation of MIMD [59], labeled in the red-dashed line. This study employs the two-step method for computing the IPD so that the calculations are based on the self-consistent results of modified FAC.

C. Electron-impact-ionization cross section

To compare the experimental results of Ref. [15], we take solid-density magnesium and calculate the electron-impact-ionization cross section of $e + 1s2s^22p^2\ ^2P_{1/2} - 1s2s^22p + 2e$ of Mg^{7+} under experimental condition, as shown in Fig. 5. First, the distorted wave function is used to describe the scattered electron and the result is shown in the black dashed line from the atomic structures of the isolated-ion boundary condition, which agrees well with the result of the scaled hydrogenic and distorted wave by Berg *et al.* Second, the atomic

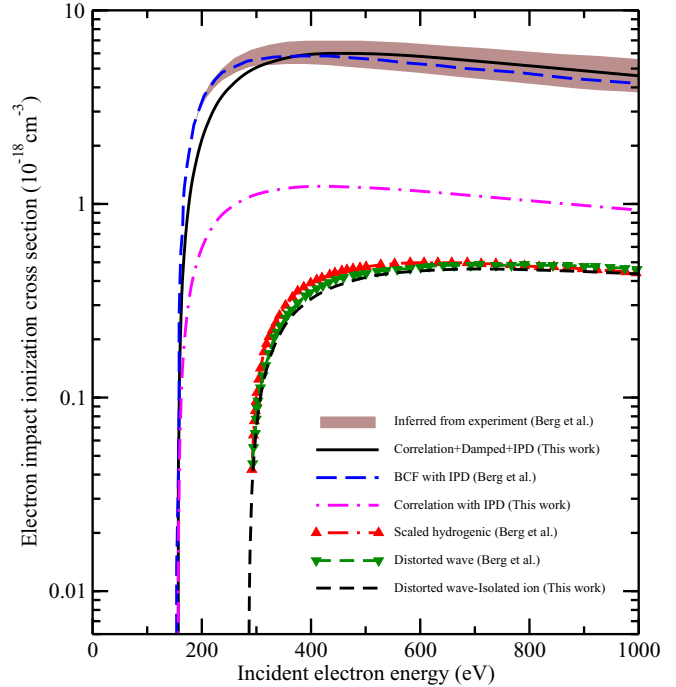


FIG. 5. Electron-impact ionization total cross-section for $e + 1s2s^22p^2\ ^2P_{1/2} - 1s2s^22p + 2e$ of Mg^{7+} , occurs in solid-density magnesium plasma at a free-electron density of $3 \times 10^{23} \text{ cm}^{-3}$ and electron temperature of 75 eV. Three methods are used to calculate the cross section, and results are compared with other theoretical calculations and experimental data of Berg *et al.* in Ref. [15].

structures calculated using the modified FAC, which includes the ionic and free-electron correlation effects, are used to consider the IPD effect when calculating the electron-impact-ionization cross sections, and the result is shown in magenta dot-dashed line. From Fig. 2, the $2p$ electron rarely changes or is affected by the effects of ionic and free-electron correlations. However, the IPD effect is noticeable and the value of Mg^{7+} from the modified FAC is 130 eV using the two-step model of Eq. (11). Also, we calculated the IPD using the SF model [58]. The results of the two models show good agreement. From Fig. 5, the effect of the IPD increases the ionization cross section, which is approximately two times that of the isolated-ion boundary condition. Based on these, we used the damped-distorted wave function [29,30] to describe the scattered electron as Eq. (10), whose result is shown as the black solid line. The result increases about one order of that of the black dashed line and is in excellent agreement with the results inferred from the theoretical BCF method and the experimental data of Berg *et al.* [15]. The damped-distorted wave function increases the overlap integral of free electrons and $2p$ electron, which strongly increases the strength of the scattering matrix. This means that the scattered decay induced by the dissipation mechanism of a warm-dense environment significantly influences the electron-impact ionization process.

IV. CONCLUSION

Conclusively, we considered the effects of the warm dense environment on the electronic structures using the

correlation functions of the ions and free electrons. The ionization potential depression (IPD) were also computed using Son's two-step model. Based on the electronic structure, the scattered-electron damping induced by the dissipative mechanism is considered by the free-electron collision frequency, which strongly enhances of the electron-impact ionization of Mg^{7+} at the free-electron density of $3 \times 10^{23} \text{ cm}^{-3}$ and temperature of 75 eV. The result is in excellent agreement with those of the theoretical BCF method and with the experimental data of Berg *et al.* [15]. The model in our calculations shed

new insights on the collisional ionization process and further aid studies on the radiation opacity of warm dense matter.

ACKNOWLEDGMENTS

This work was supported by the Science Challenge Project No. TZ2018005 and the National Natural Science Foundation of China under Grants No. 11974424, No. U1830206, and No. 11774322.

-
- [1] O. Ciricosta, S. M. Vinko, H.-K. Chung, B.-I. Cho, C. R. D. Brown, T. Burian, J. Chalupský, K. Engelhorn, R. W. Falcone, C. Graves, V. Hájková, A. Higginbotham, L. Juha, J. Krzywinski, H. J. Lee, M. Messerschmidt, C. D. Murphy, Y. Ping, D. S. Rackstraw, A. Scherz *et al.*, Direct Measurements of the Ionization Potential Depression in a Dense Plasma, *Phys. Rev. Lett.* **109**, 065002 (2012).
- [2] B. I. Cho, K. Engelhorn, S. M. Vinko, H.-K. Chung, O. Ciricosta, D. S. Rackstraw, R. W. Falcone, C. R. D. Brown, T. Burian, J. Chalupský, C. Graves, V. Hájková, A. Higginbotham, L. Juha, J. Krzywinski, H. J. Lee, M. Messerschmidt, C. Murphy, Y. Ping, N. Rohringer *et al.*, Resonant $K\alpha$ Spectroscopy of Solid Density Aluminum Plasmas, *Phys. Rev. Lett.* **109**, 245003 (2012).
- [3] T. R. Preston, S. M. Vinko, O. Ciricosta, H.-K. Chung, R. W. Lee, and J. S. Wark, The effects of ionization potential depression on the spectra emitted by hot dense aluminium plasmas, *High Energy Density Phys.* **9**, 258 (2013).
- [4] O. Ciricosta, S. M. Vinko, B. Barbrel, D. S. Rackstraw, T. R. Preston, T. Burian, J. Chalupský, B. I. Cho, H.-K. Chung, G. L. Dakovski, K. Engelhorn, V. Hájková, P. Heimann, M. Holmes, L. Juha, J. Krzywinski, R. W. Lee, S. Toleikis, J. J. Turner, U. Zastra *et al.*, Measurements of continuum lowering in solid-density plasmas created from elements and compounds, *Nat. Commun.* **7**, 11713 (2016).
- [5] D. J. Hoarty, P. Allan, S. F. James, C. R. D. Brown, L. M. R. Hobbs, M. P. Hill, J. W. O. Harris, J. Morton, M. G. Brookes, R. Shepherd, J. Dunn, H. Chen, E. Von Marley, P. Beiersdorfer, H. K. Chung, R. W. Lee, G. Brown, and J. Emig, Observations of the Effect of Ionization-Potential Depression in Hot Dense Plasma, *Phys. Rev. Lett.* **110**, 265003 (2013).
- [6] S. M. Vinko, O. Ciricosta, T. R. Preston, D. S. Rackstraw, C. R. D. Brown, T. Burian, J. Chalupský, B. I. Cho, H.-K. Chung, K. Engelhorn, R. W. Falcone, R. Fiokovinini, V. Hájková, P. A. Heimann, L. Juha, H. J. Lee, R. W. Lee, M. Messerschmidt, B. Nagler, W. Schlotter *et al.*, Investigation of femtosecond collisional ionization rates in a solid-density aluminum plasma, *Nat. Commun.* **6**, 6397 (2015).
- [7] R. P. Drake, Perspectives on high-energy-density physics, *Phys. Plasmas* **16**, 055501 (2009).
- [8] S. D. Bergeson, S. D. Baalrud, C. L. Ellison, E. Grant, F. R. Graziani, T. C. Killian, M. S. Murillo, J. L. Roberts, and L. G. Stanton, Exploring the crossover between high-energy-density plasma and ultracold neutral plasma physics, *Phys. Plasmas* **26**, 100501 (2019).
- [9] A. Müller, Electron-ion collisions: Fundamental processes in the focus of applied research, *Adv. At. Mol. Opt. Phys.* **55**, 293 (2008).
- [10] E. Landi and M. Landini, Radiative losses of optically thin coronal plasmas, *Astron. Astrophys.* **347**, 401 (1999).
- [11] P. Bryans, E. Landi, and D. W. Savin, A new approach to analyzing solar coronal spectra and updated collisional ionization equilibrium calculations. II. Additional ionization rate coefficients, *Astrophys. J.* **691**, 1540 (2009).
- [12] N. Booth, A. P. L. Robinson, P. Hakel, R. J. Clarke, R. J. Dance, D. Doria, L. A. Gizzi, G. Gregori, P. Koester, L. Labate, T. Levato, B. Li, M. Makita, R. C. Mancini, J. Pasley, P. P. Rajeev, D. Riley, E. Wagenaars, J. N. Waugh, and N. C. Woolsey, Laboratory measurements of resistivity in warm dense plasmas relevant to the microphysics of brown dwarfs, *Nat. Commun.* **6**, 8742 (2015).
- [13] S. J. Rose, New experimental possibilities for measuring radiative opacity under conditions in the Sun's interior, *Plasma Phys. Control. Fusion* **47**, B735 (2005).
- [14] R. C. Mancini, T. E. Lockard, D. C. Mayes, I. M. Hall, G. P. Loisel, J. E. Bailey, G. A. Rochau, J. Abdallah, Jr., I. E. Golovkin, and D. Liedahl, X-ray heating and electron temperature of laboratory photoionized plasmas, *Phys. Rev. E* **101**, 051201(R) (2020).
- [15] Q. Y. van den Berg, E. V. Fernandez-Tello, T. Burian, J. Chalupsky, H. K. Chung, O. Ciricosta, G. L. Dakovski, V. Hajkova, P. Hollebon, L. Juha, J. Krzywinski, R. W. Lee, M. P. Minitti, T. R. Preston, A. G. de la Varga, V. Vozda, U. Zastra, J. S. Wark, P. Velarde, and S. M. Vinko, Clocking Femtosecond Collisional Dynamics via Resonant X-Ray Spectroscopy, *Phys. Rev. Lett.* **120**, 055002 (2018).
- [16] T. R. Kallman and P. Palmeri, Atomic data for x-ray astrophysics, *Rev. Mod. Phys.* **79**, 79 (2007).
- [17] M. A. Lennon, K. L. Bell, H. B. Gilbody, J. G. Hughes, A. E. Kingston, M. J. Murray, and F. J. Smith, Recommended data on the electron impact ionization of atoms and ions: Fluorine to nickel, *J. Phys. Chem. Ref. Data* **17**, 1285 (1988).
- [18] E. Kallne and L. A. Jones, Measurements of the ionisation rates of lithium-like ions, *J. Phys. B: At. Mol. Phys.* **10**, 3637 (1977).
- [19] P. Debye and E. Hückel, The theory of electrolytes. I. The lowering of the freezing point and related occurrences, *Phys. Z* **24**, 185 (1923).
- [20] R. K. Janev, S. B. Zhang, and J. G. Wang, Review of quantum collision dynamics in Debye plasmas, *Matter Radiat. Extrem.* **1**, 237 (2016).

- [21] M. C. Zammit, D. V. Fursa, and I. Bray, Convergent-close-coupling calculations for excitation and ionization processes of electron-hydrogen collisions in Debye plasmas, *Phys. Rev. A* **82**, 052705 (2010).
- [22] C. E. Starrett and D. Saumon, Fully variational average atom model with ion-ion correlations, *Phys. Rev. E* **85**, 026403 (2012).
- [23] C. E. Starrett, D. Saumon, J. Daligault, and S. Hamel, Integral equation model for warm and hot dense mixtures, *Phys. Rev. E* **90**, 033110 (2014).
- [24] D. Saumon, C. E. Starrett, J. D. Kress, and J. Clérouin, The quantum hypernetted chain model of warm dense matter, *High Energy Density Phys.* **8**, 150 (2012).
- [25] Y. Hou, Y. Jin, P. Zhang, D. Kang, C. Gao, R. Redmer, and J. Yuan, Ionic self-diffusion coefficient and shear viscosity of high-Z materials in the hot dense regime, *Matter Radiat. Extrem.* **6**, 026901 (2021).
- [26] Y. Hou, R. Bredow, J. M. Yuan, and R. Redmer, Average-atom model combined with the hypernetted chain approximation applied to warm dense matter, *Phys. Rev. E* **91**, 033114 (2015).
- [27] Y. Hou, Y. S. Fu, R. Bredow, D. D. Kang, R. Redmer, and J. M. Yuan, Average-atom model for two-temperature states and ionic transport properties of aluminum in the warm dense matter regime, *High Energy Density Phys.* **22**, 21 (2017).
- [28] D. Sébilleau, K. Hatada, and H. Ebert, *Multiple Scattering Theory for Spectroscopies*, Springer Proceedings in Physics (Springer, Berlin, 2018), Vol. 204.
- [29] W. R. Johnson, Low-frequency conductivity in the average-atom approximation, *High Energy Density Phys.* **5**, 61 (2009).
- [30] M. Y. Kuchiev and W. R. Johnson, Low-frequency plasma conductivity in the average-atom approximation, *Phys. Rev. E* **78**, 026401 (2008).
- [31] W. R. Johnson, C. Guet, and G. F. Bertsch, Optical properties of plasmas based on an average-atom model, *J. Quant. Spectrosc. Radiat. Transfer* **99**, 327 (2006).
- [32] P. F. Liu, C. Gao, Y. Hou, J. L. Zeng, and J. M. Yuan, Transient space localization of electrons ejected from continuum atomic processes in hot dense plasma, *Commun. Phys.* **1**, 95 (2018).
- [33] M. F. Gu, The flexible atomic code, *Can. J. Phys.* **86**, 675 (2008).
- [34] S. K. Son, R. Thiele, Z. Jurek, B. Ziąja, and R. Santra, Quantum-Mechanical Calculation of Ionization-Potential Lowering in Dense Plasmas, *Phys. Rev. X* **4**, 031004 (2014).
- [35] S. H. Glenzer and R. Redmer, X-ray Thomson scattering in high energy density plasmas, *Rev. Mod. Phys.* **81**, 1625 (2009).
- [36] W. C. Dharma-Wardana and H. Taylor, Exchange and correlation potentials for finite temperature quantum calculations at intermediate degeneracies, *J. Phys. C: Solid State Phys.* **14**, 629 (1981).
- [37] R. P. Feynman, N. Metropolis, and E. Teller, Equations of state of elements based on the generalized Fermi-Thomas theory, *Phys. Rev.* **75**, 1561 (1949).
- [38] M. Thøgersen, N. T. Zinner, and A. S. Jensen, Thomas-Fermi approximation for a condensate with higher-order interactions, *Phys. Rev. A* **80**, 043625 (2009).
- [39] K. Wünsch, P. Hilse, M. Schlanges, and D. O. Gericke, Structure of strongly coupled multicomponent plasmas, *Phys. Rev. E* **77**, 056404 (2008).
- [40] R. Bredow, T. Bornath, W.-D. Kraeft, and R. Redmer, Hypernetted chain calculations for multi-component and nonequilibrium plasmas, *Contrib. Plasma Phys.* **53**, 276 (2013).
- [41] V. Schwarz, T. Bornath, W.-D. Kraeft, S. H. Glenzer, A. Höll, and R. Redmer, Hypernetted chain calculations for two-component plasmas, *Contrib. Plasma Phys.* **47**, 324 (2007).
- [42] V. Bezkrivnyy, M. Schlanges, D. Kremp, and W.-D. Kraeft, Reaction ensemble Monte Carlo technique and hypernetted chain approximation study of dense hydrogen, *Phys. Rev. E* **69**, 061204 (2004).
- [43] M. Baus and J. Hansen, Statistical mechanics of simple Coulomb systems, *Phys. Rep.* **59**, 1 (1980).
- [44] D. Kremp, M. Schlanges, and W.-D. Kraeft, *Quantum Statistics of Nonideal Plasma* (Springer, Berlin, 2005).
- [45] J. Clérouin, P. Arnault, C. Ticknor, J. D. Kress, and L. A. Collins, Unified Concept of Effective One Component Plasma for Hot Dense Plasmas, *Phys. Rev. Lett.* **116**, 115003 (2016).
- [46] Y. X. Wang, Solvable Strong-Coupling Quantum-Dot Model with a Non-Fermi-Liquid Pairing Transition, *Phys. Rev. Lett.* **124**, 017002 (2020).
- [47] J. L. Zeng, L. P. Liu, P. F. Liu, and J. M. Yuan, Role of ionization-excitation processes in the cross section for direct ionization of heavy atomic ions by electron impact, *Phys. Rev. A* **90**, 044701 (2014).
- [48] J. L. Zeng, Y. J. Li, Y. Hou, and J. M. Yuan, Ionization potential depression and ionization balance in dense carbon plasma under solar and stellar interior conditions, *Astron. Astrophys.* **644**, A92 (2020).
- [49] S.-I. Chu and W. P. Reinhardt, Intense Field Multiphoton Ionization via Complex Dressed States: Application to the H Atom, *Phys. Rev. Lett.* **39**, 1195 (1977).
- [50] V. C. Reed, P. L. Knight, and K. Burnett, Suppression of Ionization in Super-Intense Fields without Dichotomy, *Phys. Rev. Lett.* **67**, 1415 (1991).
- [51] R. Santra and L. S. Cederbaum, Non-Hermitian electronic theory and applications to clusters, *Phys. Rep.* **368**, 1 (2002).
- [52] G. Ecker and W. Kröll, Lowering of the ionization energy for a plasma in thermodynamic equilibrium, *Phys. Fluids* **6**, 62 (1963).
- [53] J. C. Stewart and K. D. Pyatt, Lowering of ionization potentials in plasmas, *Astrophys. J.* **144**, 1203 (1966).
- [54] C. Lin, G. Röpke, W. D. Kraeft, and H. Reinholz, Ionization-potential depression and dynamical structure factor in dense plasmas, *Phys. Rev. E* **96**, 013202 (2017).
- [55] G. Röpke, D. Blaschke, T. Doppner, C. Lin, W. D. Kraeft, R. Redmer, and H. Reinholz, Ionization potential depression and Pauli blocking in degenerate plasmas at extreme densities, *Phys. Rev. E* **99**, 033201 (2019).
- [56] C. Lin, Quantum statistical approach for ionization potential depression in multi-component dense plasmas, *Phys. Plasmas* **26**, 122707 (2019).
- [57] S. X. Hu, Continuum Lowering and Fermi-Surface Rising in Strongly Coupled and Degenerate Plasmas, *Phys. Rev. Lett.* **119**, 065001 (2017).
- [58] X. L. Zan, C. Lin, Y. Hou, and J. M. Yuan, Local field correction to ionization potential depression of ions in warm or hot dense matter, *Phys. Rev. E* **104**, 025203 (2021).
- [59] Y. S. Fu, Y. Hou, D. D. Kang, C. Gao, F. T. Jin, and J. M. Yuan, Multi-charge-state molecular dynamics and self-diffusion coefficient in the warm dense matter regime, *Phys. Plasmas* **25**, 012701 (2018).